

channel displays a pronounced transition-state resonance at  $E_c \sim 0.6$  kcal/mol (20, 23). Liu and co-workers (14, 30) have investigated the F/F\* + HD reaction in some detail but primarily at energies considerably above the resonance. Studies on an earlier set of PESs show that the resonance is absent in the F\* + HD channel (18), so that the influence of the resonance should be seen in the energy dependence of the F\*/F ratio.

Ultimately, we hope that one will reach a similarly good degree of agreement between experiment and theory in the investigation of non-adiabaticity in abstraction reactions of F with polyatomic targets, such as H<sub>2</sub>O (31) or CD<sub>4</sub> (32).

Our conclusion that at low collision energy the F\* reactivity becomes increasingly more efficient, relative to the BO-allowed F reaction of the ground spin-orbit state, agrees well with theoretical simulations of similar sophistication for the homologous Cl/Cl\* + H<sub>2</sub> reaction (33, 34) but contrasts with prior experimental work (35, 36). Future theoretical and experimental study of the Cl + H<sub>2</sub> reaction is necessary to reach a level of agreement similar to what we have reported here for the F + D<sub>2</sub> reaction.

#### References and Notes

- M. Born, J. R. Oppenheimer, *Ann. Phys.* **84**, 457 (1927).
- M. S. Child, *Molecular Collision Theory* (Academic, New York, ed. 2, 1974).
- L. J. Butler, *Annu. Rev. Phys. Chem.* **49**, 125 (1998).
- K. E. Shuler, *J. Chem. Phys.* **21**, 624 (1953).
- R. J. Donovan, D. Husain, *Chem. Rev.* **70**, 489 (1970).
- K. Stark, H.-J. Werner, *J. Chem. Phys.* **104**, 6515 (1996).
- M. H. Alexander, D. E. Manolopoulos, H. J. Werner, *J. Chem. Phys.* **113**, 11084 (2000).
- J. C. Tully, *J. Chem. Phys.* **60**, 3042 (1974).
- D. M. Neumark, A. M. Wodtke, G. N. Robinson, C. C. Hayden, Y. T. Lee, *J. Chem. Phys.* **82**, 3045 (1985).
- D. M. Neumark *et al.*, *J. Chem. Phys.* **82**, 3067 (1985).
- M. Faubel, B. Martinez-Haya, L. Y. Rusin, U. Tappe, J. P. Toennies, *J. Phys. Chem. A* **101**, 6415 (1997).
- S. A. Nizkorodov, W. W. Harper, D. J. Nesbitt, *Faraday Disc. Chem. Soc.* **113**, 107 (1999).
- W. W. Harper, S. A. Nizkorodov, D. J. Nesbitt, *J. Chem. Phys.* **116**, 5622 (2002).
- F. Dong, S.-H. Lee, K. Liu, *J. Chem. Phys.* **113**, 3633 (2000).
- F. Rebentrost, W. A. Lester Jr., *J. Chem. Phys.* **63**, 3737 (1975).
- F. Rebentrost, W. A. Lester Jr., *J. Chem. Phys.* **64**, 3879 (1976).
- G. C. Schatz, *J. Phys. Chem.* **99**, 7522 (1995).
- Y. R. Tzeng, M. H. Alexander, *J. Chem. Phys.* **121**, 5812 (2004).
- L. Schlieder, K. Seekamp-Rahn, E. Wrede, K. H. Welge, *J. Chem. Phys.* **107**, 6175 (1997).
- K. Liu, R. T. Skodje, D. E. Manolopoulos, *PhysChemComm* **4**, 27 (2002).
- S. A. Harich *et al.*, *Nature* **419**, 281 (2002).
- D. Dai *et al.*, *Science* **300**, 1730 (2003).
- M. Qiu *et al.*, *Science* **311**, 1440 (2006).
- Methods are detailed on Science Online. See fig. S1 for the VUV autoionization spectrum and figs. S2 and S3 for the predicted rotational distributions in DF ( $v = 2$ ) and DF ( $v = 3$ ), respectively.
- B. Ruscic, J. P. Greene, J. Berkowitz, *J. Phys. B* **17**, 179 (1984).

- R. D. Levine, R. B. Bernstein, *Molecular Reaction Dynamics and Chemical Reactivity* (Oxford Univ. Press, New York, 1987).
- M. H. Alexander, Y.-R. Tzeng, D. Skouteris, in *Chemical Reaction Dynamics*, G. Lendvay, A. Laganá, Eds. (Kluwer Academic, Amsterdam, 2004), pp. 45–65.
- E. E. Nikitin, *Theory of Elementary Atomic and Molecular Processes in Gases* (Clarendon, Oxford, 1974).
- V. Aquilanti, G. Grossi, *J. Chem. Phys.* **73**, 1165 (1980).
- S.-H. Lee, F. Dong, K. Liu, *Faraday Disc. Chem. Soc.* **127**, 49 (2004).
- M. Ziemkiewicz, M. Wojcik, D. J. Nesbitt, *J. Chem. Phys.* **123**, 224307 (2005).
- J. Zhou, W. Shiu, J. J. Lin, K. Liu, *J. Chem. Phys.* **124**, 104309 (2006).
- M. H. Alexander, G. Capecchi, H.-J. Werner, *Science* **296**, 715 (2002).
- M. H. Alexander, G. Capecchi, H.-J. Werner, *Faraday Disc. Chem. Soc.* **127**, 59 (2004).
- S.-H. Lee, L.-H. Lai, K. Liu, H. Chang, *J. Chem. Phys.* **110**, 8229 (1999).
- F. Dong, S.-H. Lee, K. Liu, *J. Chem. Phys.* **115**, 1197 (2001).
- X.Y. and D.H.Z. were supported by the Chinese Academy of Sciences, the National Natural Science Foundation of China and the Ministry of Science and Technology of China. H.J.W. was supported by the Deutsche Forschungsgemeinschaft and the Fonds der Chemischen Industrie. M.H.A. is grateful to the U.S. NSF for support under grant CHE-0413743.

#### Supporting Online Material

[www.sciencemag.org/cgi/content/full/317/5841/1061/DC1](http://www.sciencemag.org/cgi/content/full/317/5841/1061/DC1)

Materials and Methods

Figs. S1 and S2

References

11 May 2007; accepted 2 July 2007

10.1126/science.1144984

## Glaciers Dominate Eustatic Sea-Level Rise in the 21st Century

Mark F. Meier,<sup>1\*</sup> Mark B. Dyurgerov,<sup>1,2</sup> Ursula K. Rick,<sup>1,3</sup> Shad O'Neel,<sup>1,4,5</sup> W. Tad Pfeffer,<sup>1,6</sup> Robert S. Anderson,<sup>1,5</sup> Suzanne P. Anderson,<sup>1,7</sup> Andrey F. Glazovsky<sup>8</sup>

Ice loss to the sea currently accounts for virtually all of the sea-level rise that is not attributable to ocean warming, and about 60% of the ice loss is from glaciers and ice caps rather than from the two ice sheets. The contribution of these smaller glaciers has accelerated over the past decade, in part due to marked thinning and retreat of marine-terminating glaciers associated with a dynamic instability that is generally not considered in mass-balance and climate modeling. This acceleration of glacier melt may cause 0.1 to 0.25 meter of additional sea-level rise by 2100.

Disintegrating glacier ice constitutes a substantial and accelerating cause of global sea-level rise. We synthesized results from a variety of recent ice mass change studies in an effort to present a more accurate picture of changes and trends in ice volume and associated sea-level rise. This synthesis includes current results that update the Intergovernmental Panel on Climate Change (IPCC) Fourth Assessment Report (1), stresses the importance of dynamic processes in transporting terrestrial ice to the sea, compares the contributions of glaciers and ice caps with those from the ice sheets, and presents new projections of ice mass change to the end of the 21st century.

We included all glaciers and ice caps (GIC). We excluded the Greenland and Antarctic ice sheets, but included the GIC that surround and are peripheral to the great ice sheets. We focused on present-day behavior (from about 1996 to 2006) because of its critical importance to society now and its relevance for runoff and sea-level projections to the year 2100.

A primary driver of recent ice loss is the rapid retreat and thinning of marine-terminating glaciers, which are susceptible to a nonlinear dynamic instability when their beds are below sea level. The increased role of this phenomenon in delivering ice to the ocean during recent

warming has been demonstrated for ice sheet outlets (2–4) but is also important for many GIC. This instability can markedly raise the sensitivity of glaciers to climate change. It is conventionally assumed that under near-steady state conditions, the climatically controlled surface balance (inputs by snow and loss through melt) controls the geometry of an ice mass, and geometric transitions (changes in thickness) are forced by changes in surface mass balance. In contrast, under dynamically forced conditions, changes in ice velocity are forced instead by changes in subglacial mechanics, and geometric transitions are governed by changes in flux divergence rather than surface balance.

<sup>1</sup>Institute of Arctic and Alpine Research, UCB 450, University of Colorado at Boulder, Boulder, CO 80309–0450, USA.

<sup>2</sup>Department of Physical Geography and Quaternary Geology, Stockholm University, SE-1061, Stockholm, Sweden.

<sup>3</sup>Department of Atmospheric and Oceanic Sciences, UCB 311, University of Colorado at Boulder, Boulder, CO 80309–0311, USA.

<sup>4</sup>Geophysical Institute, University of Alaska-Fairbanks, Fairbanks, AK 99775–7320, USA.

<sup>5</sup>Department of Geological Sciences, UBC 399, University of Colorado at Boulder, Boulder, CO 80309–0399, USA.

<sup>6</sup>Department of Civil, Environmental, and Architectural Engineering, UCB 428, University of Colorado at Boulder, Boulder, CO 80309–0428, USA.

<sup>7</sup>Department of Geography, UCB 260 University of Colorado at Boulder, Boulder, CO 80309–0260, USA.

<sup>8</sup>Institute of Geography, Russian Academy of Sciences, Staromonetny 29, 119107, Moscow, Russia.

\*To whom correspondence should be addressed. E-mail: mark.meier@colorado.edu

The whole-glacier continuity equation for the rate of change of glacier ice mass,  $\dot{M}$ , is

$$\dot{M} = \dot{M}_b + \dot{M}_h + \dot{M}_L = \int_A \rho_i \dot{b} dA + \int_A (-\nabla q) \rho_i dA + \rho_i W_T H_T (u_T - u_c)$$

where dots denote differentiation with respect to time,  $\dot{M}_b$  is the glacier-wide net meteorological mass balance (the local surface mass balance,  $\dot{b}$ , integrated over the glacier area,  $A$ );  $\dot{M}_h$  represents average thickening or thinning associated with the local divergence of ice discharge,  $q$ , integrated over the glacier area; and  $\dot{M}_L$  represents net mass change due to extension or retraction of the terminus governed by the balance between calving at a rate  $u_c$  and terminus ice speed,  $u_T$ , at a terminus of width  $W_T$  and ice thickness  $H_T$ .  $\rho_i$  is the density of ice. The contribution of mass to the sea from a retreating tidewater glacier ( $-\dot{M}$ ) is therefore the sum of ice losses driven by meteorology ( $\dot{M}_b$ ), by draw-down of the ice reservoir due to ice dynamics ( $\dot{M}_h$ ), and by terminus dynamics ( $\dot{M}_L$ ). We report these as mass fluxes in gigatons (Gt) per year (1 Gt = mass of 1 km<sup>3</sup> water = 1/362-mm sea-level change).

For many marine-terminating outlet and tidewater glaciers, thinning and hence ice loss associated with dynamic instability can be appreciably greater than thinning caused by the local surface mass balance. Alaska's Columbia Glacier provides a useful example. Before the onset of rapid retreat around 1980, this glacier

maintained a nearly steady-state elevation profile (a robust proxy for a steady-state thickness profile), for which the positive surface mass balance, estimated at  $\dot{M}_b = 0.37$  Gt/year, was closely balanced by dynamic surface lowering. During the late 1970s, however, net thinning began to occur ( $\dot{M}_b + \dot{M}_h = -0.88$  Gt/year), portending dynamic retreat (5, 6); about 15 km of terminus retreat ensued. Columbia Glacier's discharge has since increased. In 2000 to 2001, the ice flux through the terminus reached 6.6 Gt/year even though the surface mass balance was probably decreasing (7). Arendt *et al.* (8) have pointed out the critical role of these effects in the wastage of other calving glaciers in the western Chugach Mountains, Alaska. This switch from balance-controlled to dynamically forced modes must be understood in comparing global ice-wastage observations and in predicting future delivery of glacier ice to the oceans. The time scale for extracting large volumes of ice from tidewater glaciers as well as from the margins of the major ice sheets can be notably shorter than one would predict from surface mass-balance estimates or climate-balance modeling.

Other calculations of losses due to changes in ice dynamics are rare. Studies in the Russian Arctic (Franz Josef Land, Novaya Zemlya, and Severnaya Zemlya) over the period from 1952 to 2001 estimate  $\dot{M}_L = -1.3$  Gt/year and  $\dot{M}_b + \dot{M}_h = -3.2$  Gt/year (9). Recent studies on the Devon Island Ice Cap (10) indicate that iceberg calving caused up to 30% of the mass loss between 1960 and 1999. These results suggest that, in areas where tidewater and calving glaciers occur, the errors in estimating ice loss of GIC from classic surface observations are likely to be

higher than stated because of the paucity of data on ice dynamic contributions to volume losses.

Rates of ice mass change ( $\dot{M}$ ) from 1995 to 2005 (Table 1, Fig. 1, and table S1) show accelerating rates of mass loss ( $\ddot{M} > 0$ ) from almost all glacier inventories. The rates are indexed to the common year 2006, and the current accelerations of loss in ice mass ( $\ddot{M}$ ) are obtained by linear regressions of published values of rate of mass loss versus time, beginning in 2000 or slightly before (figs. S1 to S3). These rates of ice loss include dynamically forced losses where known; because these are not known in many areas, the values reported must be considered underestimates. For comparison, we also present recent results from the Greenland and Antarctic ice sheets in Table 1 and Fig. 2. The rate of GIC ice loss ( $\pm$ SD) of  $402 \pm 95$  Gt/year dominates the contributions to sea-level rise from the various ice masses in 2006 (Table 1), and the GIC around the Gulf of Alaska contribute substantially ( $>100$  Gt/year; Fig. 1).

The recent rate of worldwide sea-level rise is about  $3.1 \pm 0.7$  mm/year; of this, ocean warming (the steric effect) accounts for about  $1.6 \pm 0.5$  mm/year (1). The results given in Table 1 suggest that glacier and ice sheet wastage currently generates 1.8 mm/year of sea-level rise, accounting for slightly more than the remainder of the nonsteric sea-level change. Our results, consistent with those in the IPCC Fourth Assessment (1), suggest that GIC contribute about 60% of the eustatic, new-water component of sea-level rise (Table 1 and Fig. 2). Our GIC wastage numbers are slightly greater than those reported in a recent consensus statement (11) prepared for the IPCC because the Fourth Assessment reports on an earlier period (1993 to 2003) and the acceleration of ice loss is very large (Fig. 1).

We explored the future effect of ice wastage for two scenarios in Table 1: (i) The present acceleration of mass loss remains constant ( $\ddot{M} =$  present value; figs. S1 to S3), and (ii) the present rate of mass loss remains constant ( $\ddot{M} =$  present value;  $\dot{M} = 0$ ). The surface mass-balance contribution to estimates of mass loss would presumably be more accurate if linked to atmospheric models incorporating changes in CO<sub>2</sub> emissions, but our emphasis is on dynamic changes to the glacier mass budget. We included only observed and documented dynamic changes in our assessment, and made no attempt to include changes that may be initiated by ice-ocean interaction in the near future. We note that dynamic adjustments can be rapid and may turn on and off asynchronously, as demonstrated in Alaska (12) and Greenland (3); one should also assume that with further warming these dynamic changes will likely accelerate. These extrapolations suggest that the GIC contribution will exceed or equal that of either ice sheet throughout at least the first half of this century, and perhaps all of this century, and will deplete at most 35% of the available GIC volume, taken here as  $250 \times 10^3$  km<sup>3</sup> water equivalent (13, 14), by 2100.

**Table 1.** Present-day rate of ice mass loss ( $\dot{M}$ ), its projected rate of change ( $\ddot{M}$ ) and rates of sea-level rise (SLR). The  $\dot{M}$  includes surface mass balance, as well as dynamic effects where known. For Greenland and Antarctica, we used published results, as in (4), but we subtracted GIC mass balances [ $-26$  to  $-50$  Gt/year (13), depending on gravity signal leakage pattern] from the Greenland gravity results to avoid double counting the GIC ice losses. We did not make this adjustment for the Antarctic because the known major changes in the Antarctic Peninsula are not necessarily reflected in the gravity results.

	$\dot{M}$ in 2006 Gt/year	$\ddot{M}$ in 2006 Gt/year <sup>2</sup>	SLR rate in 2006 mm/year	Total SLR to 2050 mm	Total SLR to 2100 mm
<b>Glaciers and ice caps</b>					
Assuming current acceleration	$-402 \pm 95$	$-11.9 \pm 5.6$	$1.1 \pm .24$	$81 \pm 43$	$240 \pm 128$
Assuming no acceleration	$-402 \pm 95$	0.0	$1.1 \pm .24$	$49 \pm 12$	$104 \pm 25$
<b>Greenland Ice Sheet</b>					
Assuming current acceleration	$-182 \pm 34$	$-16.2 \pm 6.3$	$0.5 \pm 0.1$	$65 \pm 28$	$245 \pm 106$
Assuming no acceleration	$-182 \pm 34$	0	$0.5 \pm 0.1$	$22 \pm 4$	$47 \pm 8$
<b>West Antarctic Ice Sheet</b>					
Assuming current acceleration	$-117 \pm 15$	$-7.3 \pm 3?$	$0.32 \pm 0.04$	$34 \pm 15?$	$120 \pm 50?$
Assuming no acceleration	$-117 \pm 15$	0	$0.32 \pm 0.04$	$14 \pm 2$	$30 \pm 4$
<b>East Antarctic Ice Sheet</b>					
Assuming current acceleration	$56 \pm 26$	$3.4 \pm 2?$	$-0.15 \pm 0.07$	$-16 \pm 12?$	$-56 \pm 40?$
Assuming no acceleration	$56 \pm 26$	0	$-0.15 \pm 0.07$	$-7 \pm 3$	$15 \pm 7$
<b>Global total</b>					
Assuming current acceleration	$-645 \pm 170$	$-32 \pm 10?$	$1.8 \pm 0.5$	$160 \pm 65?$	$560 \pm 230?$
Assuming no acceleration	$-645 \pm 170$	0	$1.8 \pm 0.5$	$78 \pm 21$	$167 \pm 44$

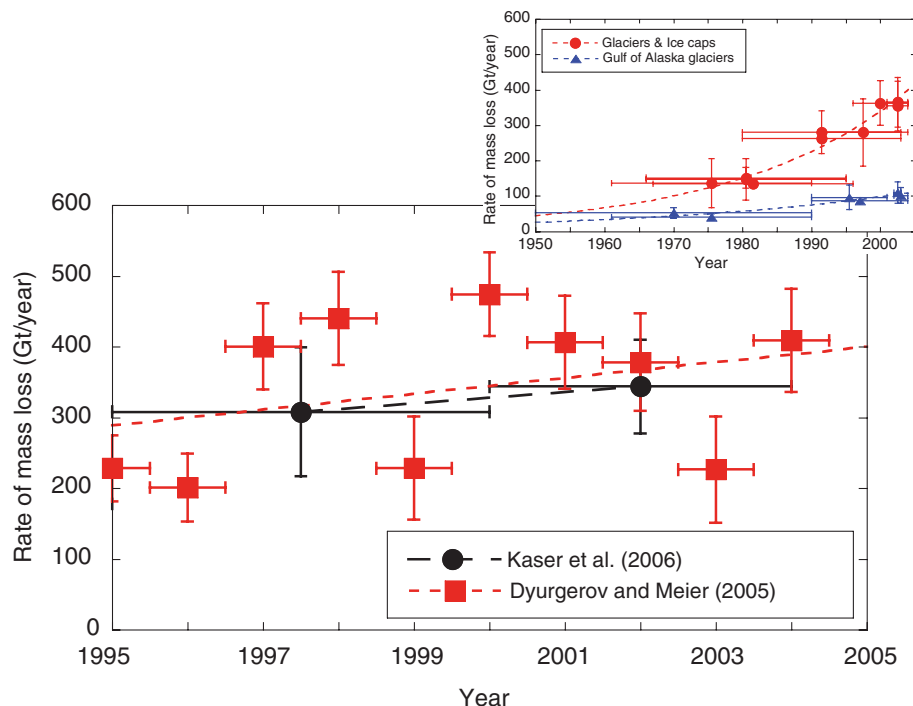


**Fig. 1.** Rate of ice mass loss from all GIC since 1995 (11, 13). Vertical error bars indicate the published uncertainty; horizontal bars show the years over which the mass balance has been averaged. (Inset) Rate of mass loss from all GIC for the period from 1950 to 2005. The red dashed curve exponential indicates the best fit through the total mass loss; the blue dashed curve applies only to the glaciers in the Gulf of Alaska. Data, method, and authorships are given in table S1.

These projections appear to be larger than those suggested by the IPCC (1), much larger than suggested by some authors [e.g., (15)], but in close agreement with other recent work (16). At the very least, our projections indicate that future sea-level rise may be larger than anticipated and that the component due to GIC will continue to be substantial.

The values suggested for the GIC contribution to rising sea-level in future years might be questioned because they do not consider the loss of glacier area. Most previous models of GIC discharge begin with a fixed “reservoir” of GIC ice that decreases in area and volume as global warming progresses. Indeed, many of the smallest glaciers are likely to vanish during the 21st century. However, (i) most of the GIC area on Earth is accounted for by a relatively few large glaciers (such as subpolar ice caps) that will not shrink appreciably in area during the 21st century; and (ii) cold glaciers in the polar regions, which do not now produce runoff to the ocean, will warm to the point where appreciable runoff to the sea can be expected.

Using a global size distribution of glaciers combined with volume, area, and thickness scaling (17, 18), we found that more than half of the ice volume in GIC is contained in ice masses that are individually >4000 km<sup>2</sup>, with mean thicknesses of ≈300 m (19). The current average global thinning rate of all GIC is about 0.55 m (ice equivalent)/year and is increasing at about 0.0164 m/year<sup>2</sup> (Table 1). Total projected thin-

ning by the year 2100 is only 50 and 120 m for steady and accelerating wastage scenarios, respectively. Although this is heartening, the median area of 34 “benchmark glaciers,” which have time series of glacier mass balance since the 1960s, is only 4.18 km<sup>2</sup>, corresponding to a mean thickness of a few tens of meters (~60 m). Thus many of these will likely disappear along with their valuable long-term records.

Our estimates include many possible errors, including measurement errors and area uncertainties, which are difficult to quantify but are likely only a few percent of the global totals. Our neglect of warming of polar firm and subsequent runoff, and of both mass balance–altitude feedback and ill-understood dynamic instabilities, leads to underestimation of sea-level rise. Neglecting area losses and ignoring the density change correction for ice removed from below sea-level produce small overestimates. Total errors (Table 1) do not significantly affect our conclusions.

To improve our understanding of the ice melt contribution to sea level, we must recognize that the GIC, not the big ice sheets, are most important today, and will continue to be important throughout this century. Complex processes driving the behavior of glaciers need better characterization. With the growing emergence of dynamically forced thinning and retreat as a dominant mass-loss process on both calving glaciers and ice sheet outlets, rates of volume change have become very nonsteady. Studies of retreat-

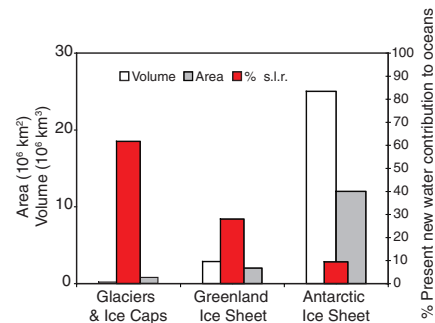


**Fig. 2.** Contributions of GIC, Greenland, and Antarctic Ice Sheets to present-day rate of sea-level rise (s.l.r.), along with their respective volumes and areas.

ing tidewater glaciers, completed and under way, are very helpful in understanding the analogous phenomenon at ice sheet outlet streams. The GIC around the edges of the big ice sheets, with total area estimated to be more than  $200 \times 10^3$  km<sup>2</sup>, require detailed examination. Spatial extrapolation to obtain regional averages for representative samples, as well as temporal extrapolation to predict future behavior, requires better knowledge of statistical distributions of glacier area and volume. Glacier volume scales nonlinearly with area, thus global grids (e.g., 1° by 1°) must be applied with great care to avoid dividing glacier areas into pieces that do not scale correctly for thickness (20).

Ice wastage contributions to sea-level rise will likely continue to increase in the future as warming of cold polar and subpolar glaciers continues and dynamically forced responses continue to occur. Our results suggest a sea-level rise of about 0.1 to 0.25 m in this century due to GIC wastage alone. This range can be compared with the IPCC projection total sea-level rise (all sources) of about 0.2 to 0.5 m depending on the emission scenario (the full effects of changes in ice sheet flow are not included). Although large ice masses may surpass the glacier contribution to sea-level rise in the distant future, the GIC contribution is important now and will be for the remainder of this century.

**References and Notes**

1. IPCC, *Climate Change 2007: The Physical Basis: Summary for Policymakers* (IPCC Secretariat, *clo* World Meteorological Organization, Geneva, 2007).
2. E. Rignot, P. Kanagaratnam, *Science* **311**, 986 (2006).
3. I. M. Howat, I. R. Joughin, T. A. Scambos, *Science* **315**, 1559 (2007).
4. A. Shepherd, D. Wingham, *Science* **315**, 1529 (2007).
5. M. F. Meier *et al.*, *U.S. Geol. Surv. Open-File Rep. 80-582* (1980), pp. 1–47.
6. *U.S. Geol. Surv. Prof. Pap. 1258A to U.S. Geol. Surv. Prof. Pap. 1258H* (1982 to 1989).
7. S. O’Neel, W. T. Pfeffer, R. Krimmel, M. Meier, *J. Geophys. Res.* **110**, F03012 (2005).
8. A. Arendt *et al.*, *J. Geophys. Res.* **111**, F03019 (2006).
9. A. F. Glazovsky, Yu. Ya. Macheret, in *Glaciation of North and Central Eurasia at Present Time*, V. M. Kotlyakov, Ed. (Institute of Geography of the Russian Academy of Science, Nauka, Moscow, 2006).

10. D. O. Burgess, M. J. Sharp, D. W. F. Mair, J. A. Dowdeswell, T. J. Benham, *J. Glaciol.* **51**, 219 (2005).
11. G. Kaser, J. G. Cogley, M. B. Dyurgerov, M. F. Meier, A. Ohmura, *Geophys. Res. Lett.* **33**, L19501 (2006).
12. M. F. Meier, A. Post, *J. Geophys. Res.* **92**, 9051 (1987).
13. M. B. Dyurgerov, M. F. Meier, *Occasional Paper No. 58*, (Institute of Arctic and Alpine Research, Univ. of Colorado, Boulder, CO, 2005).
14. We have revised the total area of GIC from  $785 \times 10^3$  km<sup>2</sup> to  $763 \times 10^3$  km<sup>2</sup> because of an overestimate of the glaciers peripheral to Greenland Ice Sheet. This adjustment has been applied throughout.
15. S. C. B. Raper, R. J. Braithwaite, *Nature* **439**, 311 (2006).
16. S. Rahmstorf, *Science* **315**, 368 (2007).
17. D. B. Bahr, M. F. Meier, *Water Resour. Res.* **36**, 495 (2000).
18. D. B. Bahr, *Water Resour. Res.* **33**, 1669 (1997).
19. Because there are many areas without complete inventories of GIC sizes, we used two estimation processes to fill gaps. First, we used an estimate of the probability of the number of glaciers greater than a certain area versus that area, based on percolation theory and on known size distribution relations. The error in this process for a global total was estimated at about 13% (13). Next, we estimated the thickness of GIC based on power-law scaling with glacier area. Without sufficient independent data, it is difficult to estimate the error in the method. We estimated that the error in calculating thicknesses and thus volumes from area values is on the order of 25% for global aggregates (13) but far greater, on the order of 50%, for individual ice masses.
20. M. F. Meier, D. B. Bahr, M. B. Dyurgerov, W. T. Pfeffer, *Geophys. Res. Lett.* **32**, L17501 (2005).
21. This work was supported by NSF grants OPP 0327345, OPP 0425488, and EAR 0549566; NASA grants NGT5-155 and NAG5-13691; and a Marie Curie International Fellowship within the 6th European Community Framework Program. We thank three anonymous reviewers for their critical reading of the manuscript.

#### Supporting Online Material

www.sciencemag.org/cgi/content/full/1143906/DC1  
Figs. S1 to S3  
Table S1  
References

17 April 2007; accepted 10 July 2007  
Published online 19 July 2007;  
10.1126/science.1143906  
Include this information when citing this paper.

# The Southern Ocean Biological Response to Aeolian Iron Deposition

Nicolas Cassar,<sup>1\*</sup> Michael L. Bender,<sup>1</sup> Bruce A. Barnett,<sup>1</sup> Songmiao Fan,<sup>2</sup> Walter J. Moxim,<sup>2</sup> Hiram Levy II,<sup>2</sup> Bronte Tilbrook<sup>3</sup>

Biogeochemical rate processes in the Southern Ocean have an important impact on the global environment. Here, we summarize an extensive set of published and new data that establishes the pattern of gross primary production and net community production over large areas of the Southern Ocean. We compare these rates with model estimates of dissolved iron that is added to surface waters by aerosols. This comparison shows that net community production, which is comparable to export production, is proportional to modeled input of soluble iron in aerosols. Our results strengthen the evidence that the addition of aerosol iron fertilizes export production in the Southern Ocean. The data also show that aerosol iron input particularly enhances gross primary production over the large area of the Southern Ocean downwind of dry continental areas.

The rate of organic matter export from the surface waters of the Southern Ocean has an important impact on distributed properties of the environment. First, it influences the residual nutrient burden of waters that flow northward in the subsurface to supply nutrients to much of the extrapolar ocean (1). Second, carbon export removes CO<sub>2</sub> from surface waters, thereby influencing the atmospheric CO<sub>2</sub> concentration over both glacial-interglacial and anthropogenic time scales. There is compelling evidence that iron supply from a number of sources (such as coastal sediments, aerosols, upwelling, ice melting, and enhanced mixing over high topography) influences rates of both gross production and carbon export by Southern Ocean ecosystems. Ocean color data, for example, show that biomass is elevated downwind of aeolian iron sources, and extraordinary “patch” experiments have shown that iron addition enhances primary production

and new production in several representative regions (2).

To understand the potential for aeolian iron fertilization, we compared a large number of net community production (NCP) measurements in the Southern Ocean (3, 4) to a modeled Fe deposition (5). NCP and gross primary production (GPP) are calculated as the production rates required to maintain the observed biological O<sub>2</sub> supersaturation (derived from O<sub>2</sub>/Ar) and O<sub>2</sub> triple-isotope anomaly against equilibration by gas exchange (parameterized in terms of wind speed) (6). NCP from O<sub>2</sub> is the stoichiometrically equivalent rate of organic carbon production in excess of respiration; it approximates carbon export from the mixed layer. Our data set establishes the pattern of this fundamental rate process in the Southern Ocean at a scale heretofore accessed only for chlorophyll, which reflects biomass. We implemented these methods with samples of water from the upper-ocean mixed layer. Samples were collected by us or collaborators on cruises of opportunity and returned to the laboratory for analysis; in this way, it was possible to assemble a very large data set.

Our approach to determining NCP and GPP has distinct attributes and limitations. The method accesses production over times on the order of 1 week, corresponding to the mixed-layer depth divided by the piston velocity. We as-

sumed steady-state mixed-layer depth and productivity (clearly a simplification). We ignored exchange between the mixed-layer and underlying waters. The analysis of Wang *et al.* (7) suggests that, in the Polar Front Zone and the Subantarctic Zone, this process is of minor importance in the summer and in the spring. When the flux of O<sub>2</sub> is into the ocean, we report negative values of NCP. Although we refer to the air-sea biological O<sub>2</sub> flux as NCP, we were unable to determine whether negative values reflect net heterotrophy in the mixed layer or upwelling of O<sub>2</sub>-undersaturated waters.

Figure 1 shows summer NCP values superimposed on Southern Ocean properties (8). Most of the Southern Ocean can be considered a high-nutrient low-chlorophyll region, with the caveat that the area north of the Antarctic Polar Front (APF) is depleted in silicate during summertime. The strong westerlies around the Antarctic continent drive a northward Ekman transport of nutrient-rich circumpolar deep waters that upwell south of the APF. From the south, the Antarctic Zone lies between the Southern Boundary of the Antarctic circumpolar current and the APF, the Polar Frontal Zone stretches from the APF to the Subantarctic Front, and the Subantarctic Zone extends from the Subantarctic Front to the Subtropical Front. The Subtropical Front is the boundary between the warm and salty subtropical waters and the relatively cooler and fresher waters of the Southern Ocean. The summertime chlorophyll distribution is shown by the background colors of the map (Fig. 1).

We observed that, in general, NCP rises toward the north (Figs. 1 and 2), with considerable spatial heterogeneity. Visual inspection, along with the statistical analysis of Reuer *et al.* (4), shows that NCP is weakly correlated with climatological satellite chlorophyll estimates. Our results also show higher NCP and GPP in the spring than in the summer over most of the Southern Ocean (9) (Fig. 2). Our approach underestimates NCP in upwelling areas, where mixing to the surface of O<sub>2</sub>-depleted waters lowers the biological O<sub>2</sub> supersaturation. For this reason, the apparent poleward decrease in NCP could partially be driven by upwelling of upper circum-

<sup>1</sup>Department of Geosciences, Princeton University, Princeton, NJ 08544, USA. <sup>2</sup>Geophysical Fluid Dynamics Laboratory/National Oceanic and Atmospheric Administration, Post Office Box 308, Princeton, NJ 08542, USA. <sup>3</sup>Commonwealth Scientific and Industrial Research Organisation (CSIRO) Marine and Atmospheric Research and Antarctic Climate and Ecosystem Cooperative Research Center, Hobart, Tasmania 7001, Australia.

\*To whom correspondence should be addressed. E-mail: ncassar@princeton.edu